ACS APPLIED MATERIALS & INTERFACES

RESEARCH ARTICLE

www.acsami.org

Mechanism of Li Adsorption on Carbon Nanotube-Fullerene Hybrid System: A First-Principles Study

Wonsang Koh,[†,‡] Ji Il Choi,[†] Kevin Donaher,[§] Seung Geol Lee,[†] and Seung Soon Jang*[,†]

[†]School of Materials Science and Engineering, Georgia Institute of Technology, 771 Ferst Drive NW, Atlanta, Georgia 30332-0245, United States

[‡]School of Physics, Georgia Institute of Technology, 837 State Street, Atlanta, Georgia 30332-0430, United States

[§]Department of Applied Physics and Applied Mathematics, Columbia University, New York, New York 10027, United States

Supporting Information

ABSTRACT: The lithium (Li) adsorption mechanism on the metallic (5,5) single wall carbon nanotube (SWCNT)-fullerene (C_{60}) hybrid material system is investigated using first-principles method. It is found that the Li adsorption energy (−2.649 eV) on the CNT-C_{60} hybrid system is lower than that on the peapod system (−1.837 eV) and the bare CNT (−1.720 eV), indicating that the Li adsorption on the CNT-C_{60} hybrid system is more stable than on the peapod or bare CNT system. This is due to the C_{60} of high electron affinity and the charge redistribution after mixing CNT with C_{60}. In order to estimate how efficiently Li can utilize the vast surface area of the hybrid system for increasing energy density, the Li adsorption energy is calculated as a function of the adsorption positions around the CNT-C_{60} hybrid system. It turns out that Li preferably occupies the mid-space between C_{60} and CNT and then wraps up the C_{60} side and subsequently the CNT side. It is also found that the electronic properties of the CNT-C_{60} system, such as band structure, molecular orbital, and charge distribution, are influenced by the Li adsorption as a function of the number of Li atoms. From the results, it is expected that the CNT-C_{60} hybrid system has enhanced the charge transport properties in addition to the Li adsorption, compared to both CNT and C_{60}.

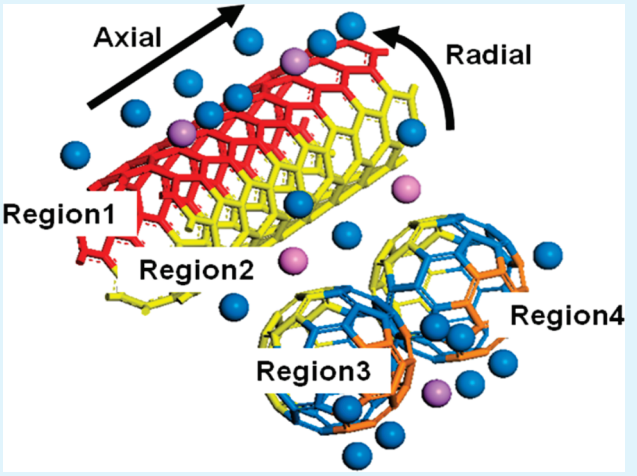

KEYWORDS: carbon nanotubes, fullerenes, hybrid carbon material, Li adsorption mechanism, density functional theory

1. INTRODUCTION

Carbon allotropes, such as fullerene (C_{60}), carbon tubes (CNTs), and graphene, have gained a great deal of attention in both science and engineering due to their extraordinary electronic and mechanical properties, leading to many applications in nanotechnology, such as field-effect transistor, composite material, and gas sensors.[1−4] In particular, it is noticed that high performance electrical energy devices such as batteries based on CNTs or their hybrid materials have been developed to promote Li adsorption, which is motivated by increasing demand for better electrochemical materials of higher energy and power density.[5]

Currently, graphitic carbon anodes have been widely adapted for the Li ion battery application due to their cycle efficiency and safety, even though metallic Li anode systems have been shown to have better Li capacity than carbon-based anodes.[6] In this context, carbon nanotubes (CNTs) have been studied both theoretically and experimentally[10−12] in order to increase the Li adsorption capacity for electrode applications because CNTs provide a vast surface area for Li adsorption as well as the above-mentioned outstanding electrical and mechanical properties.[7−9] Early studies were focused on the adsorptions of Li on the outside single-wall carbon nanotubes (SWCNTs) and multi-wall carbon nanotubes (MWCNTS) with various diameters and chiralities,[13−20] but later studies have been extended to the diffusion of Li on the interior and exterior of the CNT.[21−25] However, the experimental results of the Li intercalation on the bare CNT system have shown only slight increases of reversible capacities over that of the graphitic carbon material, which has been ascribed to the weak adsorption of Li on CNTs.[12,26,27] Hence, further development has sought to obtain strong Li adsorption through various modifications such as doping impurities, forming structural defects, and mixing with other carbon-based materials.[28−37] For instance, Shimoda et al. have reported increases in the maximum capacity (∼1000 mAh/g) of $Li_{2.7}C_6$ for SWCNTs by intercalating Li into the inside of CNTs through chemical etching of the CNTs.[30,31]

Among those modification methods aiming to improve electrochemical properties, diverse studies of carbon hybrid system

Received: January 6, 2011
Accepted: March 28, 2011
Published: March 28, 2011

Table 1. Li adsorption Energy and Charge Distribution (Mulliken Charge) of Various CNT-C_{60} Hybrid Systems

system	adsorption energy (eV)	charges (e)		
		Li	CNT	C_{60}
(5,5) CNT-C_{60} hybrid[a]	N/A	N/A	0.096	−0.096
(10,10) CNT-C_{60} hybrid	N/A	N/A	0.102	−0.102
(4,4) CNT-C_{60} hybrid	N/A	N/A	0.089	−0.089
(10,10) CNT-C_{60} peapod	N/A	N/A	0.225	−0.225
Li@(5,5) hybrid_CNT@hybrid[a]	−1.802	0.844	−0.640	−0.204
Li@(5,5) hybrid_CNT:C_{60} middle	−2.571	0.950	−0.414	−0.536
Li@(5,5) hybrid_C_{60}@hybrid[a]	−2.110	0.825	−0.020	−0.805
Li@(10,10) hybrid_CNT@hybrid	−1.740	0.846	−0.665	−0.151
Li@(10,10) hybrid_ CNT:C_{60} middle	−2.573	0.940	−0.414	−0.526
Li@(10,10) hybrid_C_{60}@hybrid	−2.106	0.823	−0.007	−0.816
Li@(4,4) hybrid_ CNT@hybrid	−1.822	0.842	−0.648	−0.194
Li@(4,4) hybrid_ CNT:C_{60} middle	−2.591	0.973	−0.454	−0.519
Li@(4,4) hybrid_C_{60}@hybrid	−2.110	0.820	−0.003	−0.817
Li@(10,10) peapod	−1.837	0.862	−0.519	−0.343
Li@(10,10) peapod	−1.835	0.858	−0.511	−0.347

[a] Ref 48.

between different carbon-base materials have also been actively attempted. In a recent study, Kawasaki et al. prepared the peapod structure by encapsulating fullerenes (C_{60}s) into the inside of SWCNTs and achieved an improvement in reversible capacities compared to the bare SWCNTs.[35] In addition, Kaneko and his coworkers could have successfully produced the SWCNT-C_{60} mixed system through the sonication of SWCNTs and C_{60}s in the toluene solution.[32] Meanwhile, Kauppinen and his coworkers synthesized another form of the CNT-C_{60} hybrid structure, called nanobuds, by covalently bonding C_{60}s to the outer surface of CNT and measured its field-emission properties, which can be utilized as a light-emission device.[36,37] Moreover, C_{60}-SWCNT complexes were used to enhance the performance of the polymer photovoltaic cells by exploiting the electron accepting property of the C_{60}.[38−40] Hence, it should be very desirable to understand the electronic properties of the CNT-C_{60} hybrid system in order to develop working devices.

In this study, we focus on the mechanism of the Li adsorption on the CNT-C_{60} hybrid system consisting of metallic SWCNTs and semiconducting C_{60} because this hybrid structure provides a simpler method for increasing Li capacity. Indeed, in our previous study, we found that the CNT-C_{60} hybrid system achieves a significant improvement in the Li adsorption compared to the bare CNT due to the higher electron affinity of C_{60}. Thus, it is very important to examine how efficiently Li atoms can utilize the vast amount of surface area on the CNT-C_{60} hybrid system.

Here, we use the first-principles computational method to study the mechanism of the Li adsorption around the CNT-C_{60} system. The Li adsorption mechanism can be investigated in detail by calculating the Li adsorption energy on the various regions around the CNT-C_{60} system and the accompanying change in the electronic properties, such as band structure, molecular orbital, and charge distribution, as a function of Li adsorption.

2. COMPUTATIONAL METHODS

In this work, the generalized gradient approximation (GGA) Perdew-Burke-Ernzerhof (PBE) functional[41,42] was employed to calculate the electron exchange-correlation energy. All the DFT calculations were performed using a double numerical basis set with d-polarization functions (DND) through DMol^3 from Accelrys.[43,44]

We chose metallic (5,5) SWCNT rather than semiconducting CNT because we are interested in its electron conduction capability as well as its appropriate size for DFT calculation. The unit cell dimensions were set to 35 Å × 35 Å × 9.846 Å to make sure that there was no direct interaction between the original structure and its self-images though the periodic boundary in the a- and b-axes, while the c-axis dimension was determined by the length of the CNT. The Monkhorst-Pack k-point scheme[45] was used for k-point sampling to determine the adsorption energy and other electronic properties, such as band structure, density of states, and Mulliken charge distribution.[46,47] We first performed the geometry-optimization of the m-(5,5) SWCNTs−Li and the CNT−C_{60}−Li system at various k points in order to determine an appropriate k-point set, and we then chose (1 × 1 × 4) k-points to examine all the properties because the change in the Li adsorption energy as a function of the k-point set became stable beyond (1 × 1 × 4) k-points.[48] The adsorption energy per Li atom on the CNT-C_{60} hybrid system ($\Delta E_{\text{adsorption}}$) was defined as

$$\Delta E_{\text{adsorption}} = \frac{E[n\text{Li} + \text{hybrid system}] - (E[\text{hybrid system}] + n \times E[\text{Li}])}{n} \quad (1)$$

where n is the number of the Li atoms, $E[n\text{Li} + \text{hybrid system}]$, $E[\text{hybrid}]$, and $E[\text{Li}]$ are the energy of the Li-adsorbed CNT-C_{60} system, the energy of the system without Li, and the energy of the single Li in vacuum, respectively. Please note that, according to this definition, the negative value of the adsorption energy indicates a favorable Li adsorption, whereas the adsorption is not favorable if the adsorption energy has a positive value. The calculated adsorption energies and electronic properties of the CNT-C_{60} system were compared to analyze the property changes as a function of the number of Li atoms in different regions.

3. RESULTS AND DISCUSSION

3.1. Single Li Atom on CNT-C_{60} Hybrid System. In order to understand the structure and properties of the CNT-C_{60} hybrid system, we fully optimized the geometry of the hybrid system

before arranging the Li atoms. The optimized structure and corresponding electronic properties, such as band structure, DOS, and charge distribution, are presented in another paper.[48] On the basis of the band structure and DOS, we concluded that

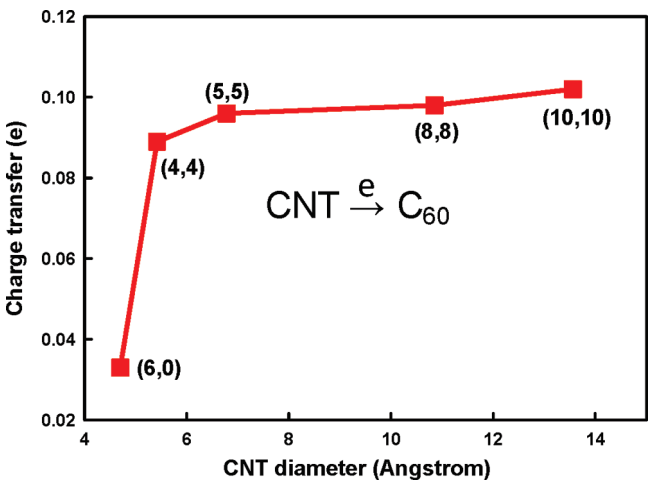

Figure 1. Charge transfer (e) from CNT to C_{60} as a function of the CNT diameter.

the whole hybrid system is metallic due to the metallic (5,5) SWCNT, but it still maintains the characteristics of each individual component. We also observed that the charge transfer occurs from CNT to C_{60} due to the relatively strong electron affinity of C_{60} whose amount was $|0.096|e$ (Table 1) calculated from the Mulliken population analysis.[48] Hence, it was concluded that the charge redistribution could impart better Li adsorption capability to the hybrid system compared with the bare CNT system.

In this study, we investigated several other CNT-C_{60} hybrid systems (metallic (4,4) CNT-C_{60}, (10,10) CNT-C_{60} hybrid system, and (10,10) CNT-C_{60} peapod system) to assess the effects of CNT diameters and configuration characteristics. As displayed in Table 1, the charge transfers on the (4,4) CNT-C_{60} and on the (10,10) CNT-C_{60} hybrid systems show a slight decrease ($|0.089|e$) and increase ($|0.102|e$), respectively, compared to the (5,5) CNT-C_{60} hybrid system, which indicates that the charge transfer depends on the diameter of CNT as displayed in Figure 1, indicating that the $\pi-\pi$ interaction can be further developed as the curvature decreases.

Although the Li adsorption energy (−1.837 eV) of the peapod is lower than that of the CNT side of the CNT-C_{60} hybrid system (CNT@hybrid) (−1.802 eV/−1.740 eV/−1.822 eV), it should be noted that the overall Li adsorption on the CNT-C_{60} hybrid systems, especially the mid-space between CNT and C_{60} (CNT:

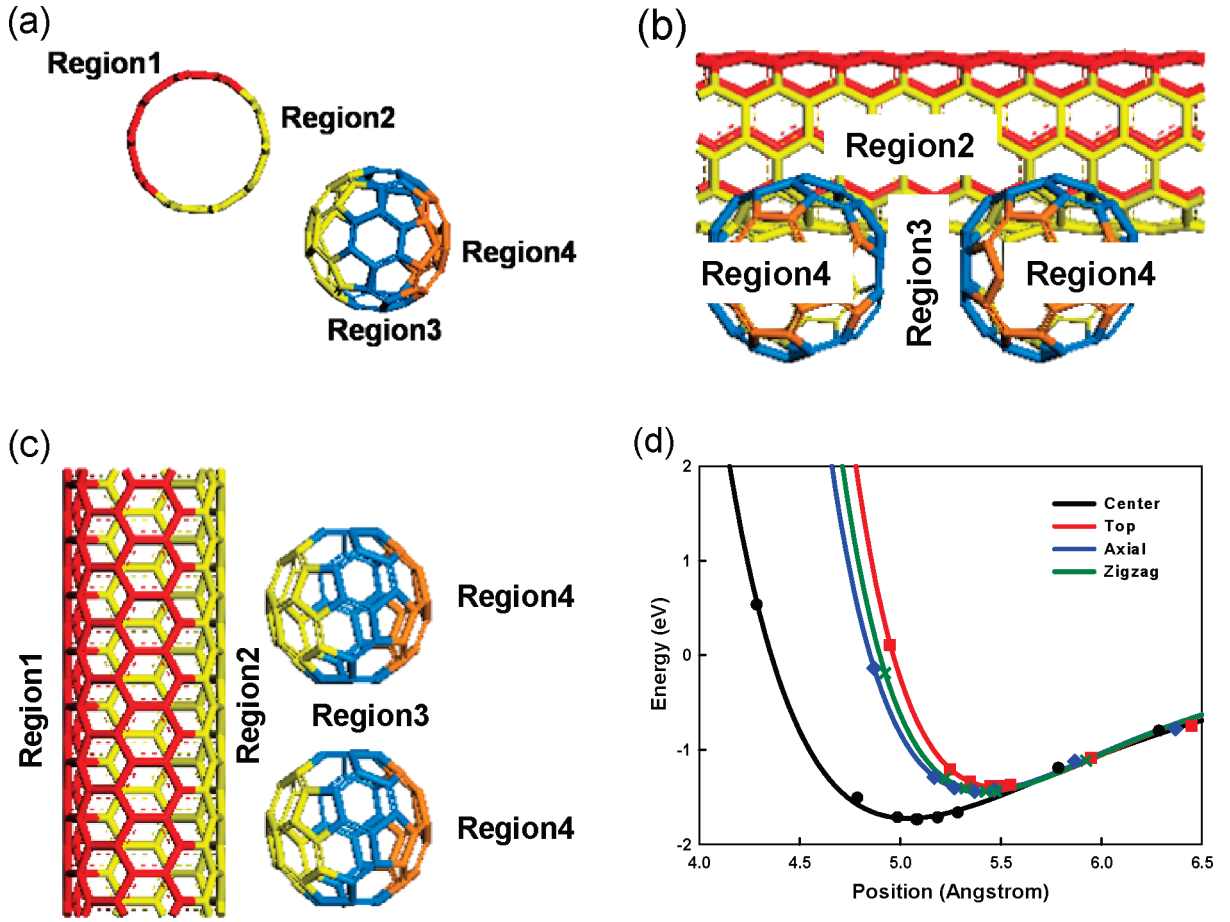

Figure 2. Basic structure of the (5,5) CNT-C_{60} hybrid system with different regions: (a) front view; (b) side view; (c) top view; region1-red, region2-yellow, region3-blue, and region4-orange; (d) Single point energy calculation of the Li atom on the different positions of the hexagonal ring in the (5,5) SWCNT of the function of the distance from the center of the SWCNT: center, top, axial, zigzag.

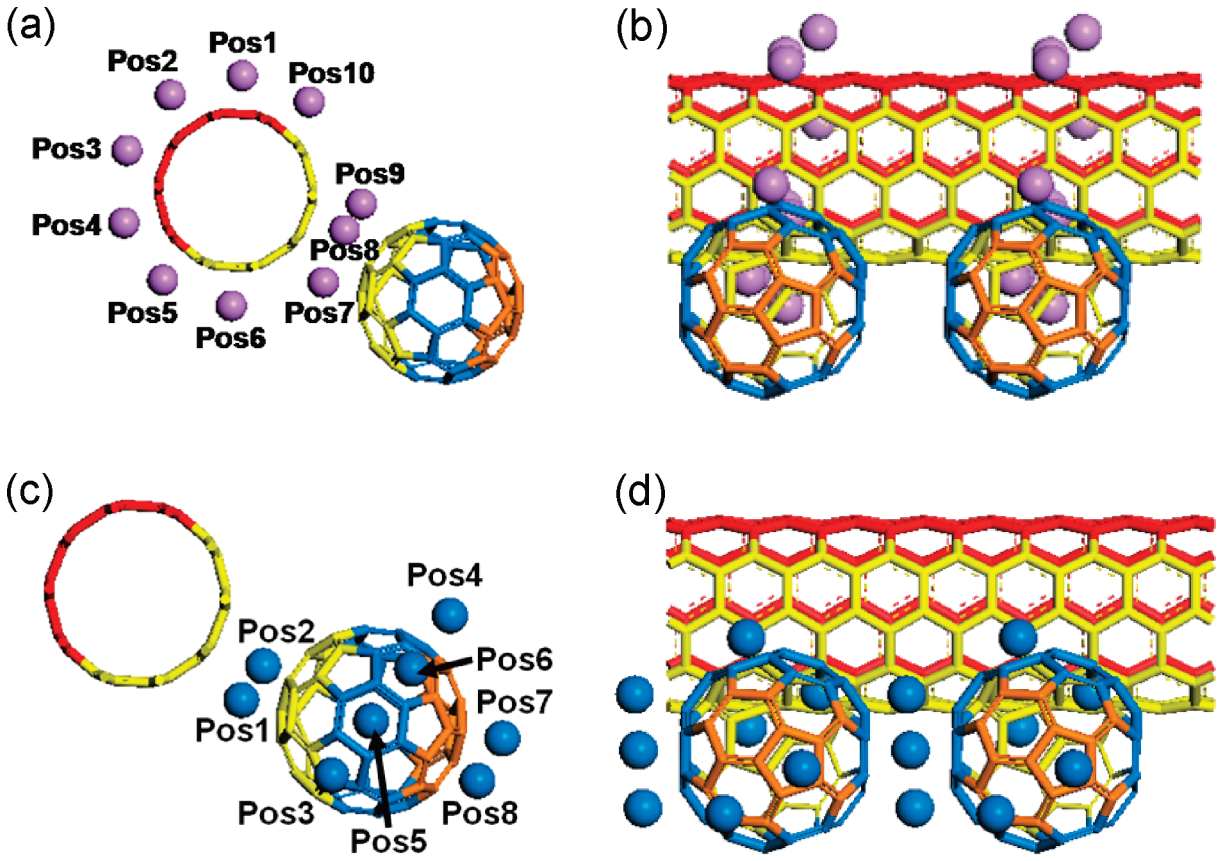

Figure 3. One-Li adsorption on various positions around CNT@hybrid: (a) front view, (b) side view; around C_{60}@hybrid: (c) front view, (d) side view.

Table 2. Adsorption Energy and Charge Distribution (Mulliken Charge) of One-Li Atom Systems

		charges		
system	adsorption energy (eV)	Li	CNT	C_{60}
1 Li on CNT(5,5)[a]	−1.720	0.835	−0.835	N/A
Pos1_CNT@hybrid (region1)[a]	−1.802	0.844	−0.640	−0.204
Pos2_CNT@hybrid (region1)	−1.797	0.844	−0.644	−0.200
Pos3_CNT@hybrid (region1)	−1.801	0.844	−0.649	−0.195
Pos4_CNT@hybrid (region1)	−1.799	0.844	−0.648	−0.196
Pos5_CNT@hybrid (region1)	−1.809	0.844	−0.634	−0.210
Pos6_CNT@hybrid (region2)	−1.859	0.852	−0.600	−0.252
Pos7_CNT@hybrid (region2)	−2.558	0.902	−0.287	−0.615
Pos8_CNT@hybrid (region2)	−2.571	0.950	−0.414	−0.536
Pos9_CNT@hybrid (region2)	−2.471	0.853	−0.333	−0.520
Pos10_CNT@hybrid (region2)	−1.829	0.847	−0.620	−0.227
1 Li on (111) Surface of C_{60} fcc[a]	−2.256	0.848	N/A	−0.848
Pos1_C_{60}@hybrid (region2_pentagon)	−2.569	0.904	−0.274	−0.630
Pos2_C_{60}@hybrid (region2_hexagon)	−2.576	0.975	−0.294	−0.681
Pos3_C_{60}@hybrid (region3_pentagon1)	−2.624	0.86	0.024	−0.884
Pos4_C_{60}@hybrid (region3_pentagon2)	−2.111	0.828	−0.032	−0.796
Pos5_C_{60}@hybrid (region3_hexagon1)	−2.514	1.484	0.045	−1.529
Pos6_C_{60}@hybrid (region3_hexagon2)	−2.649	0.863	0.026	−0.889
Pos7_C_{60}@hybrid (region4_pentagon) [a]	−2.110	0.825	−0.020	−-0.805
Pos8_C_{60}@hybrid (region4_hexagon) [a]	−2.108	0.847	−0.016	−0.831

[a] Ref 48.

Table 3. Energy Decomposition Analysis for One-Li Systems

system	adsorption energy (eV)	Es[a] (eV)	E_{NES}[b] (eV)
Pos3_CNT@hybrid (region1)	−1.801	−2.514	0.713
Pos8_CNT@hybrid (region2)	−2.571	−4.042	1.471
Pos2_C_{60}@hybrid (region2_hexagon)	−2.576	−4.134	1.558
Pos6_C_{60}@hybrid (region3_hexagon2)	−2.649	−3.090	0.441
Pos7_C_{60}@hybrid (region4_pentagon)	−2.108	−2.588	0.480

[a] Es: electrostatic energy. [b] E_{NES}: nonelectrostatic energy.

Table 4. Adsorption Energy of Many Li Adsorption Systems

system	adsorption energy (eV)
2 Li on region1: Radial (N.N.N.[a] site)[b]	−1.670
2 Li on region1: Radial (N.N.[c] site)[b]	−1.523
2 Li on region1: Axial (N.N.N. site)	−1.529
2 Li on region1: Axial (N.N. site)	−1.381
2 Li on region2 (CNT): Radial (N.N.N. site)	−2.188
2 Li on region2 (CNT): Radial (N.N. site)	−2.405
2 Li on region2 (CNT): Axial (N.N.N. site)	−2.456
2 Li on region2 (CNT): Axial (N.N. site)	−2.475
2 Li on region2 (C_{60}): Radial (N.N.N. site)	−2.297
2 Li on region2 (C_{60}): Radial (N.N. site)	−2.195
2 Li on region2 (C_{60}): Axial (N.N.N. site)	−2.632
2 Li on region2 (C_{60}): Axial (N.N. site)	−2.475
2 Li on region3: Radial (N.N.N. site)	−2.601
2 Li on region3: Radial (N.N. site)	−2.623
2 Li on region4: Radial (N.N.N. site)	−2.014
2 Li on region4: Radial (N.N. site)[b]	−1.864
2 Li on region4: Axial (N.N.N. site)[b]	−2.312
2 Li on region4: Axial (N.N. site)	−1.839
20 Li atoms on CNT@hybrid	−1.745
12 Li atoms on C_{60}@hybrid	−2.147
32 Li atoms on CNT-C_{60} hybrid	−1.809
Li−Li (experiment)	−1.030[49,50]
Li−Li (theory:Dmol^3)[b]	−1.008

[a] N.N.N.: next nearest neighbor. [b] Ref 48. [c] N.N.: nearest neighbor.

C_{60} middle) and the C_{60} side (C_{60}@hybrid), is stronger than the Li adsorption on the peapod system (Table 1). Hence, the CNT-C_{60} hybrid system would be very promising for electrode purposes because of the improved Li adsorption capability around the electrode.

To describe the Li adsorption mechanism on the CNT-C_{60} hybrid system systematically, we defined four distinct regions around the hybrid system before positioning the Li atoms as shown in the Figure 2a−c: (i) CNT side (region1, red), (ii) between CNT and C_{60} (region2, yellow), (iii) between C_{60}s (region3, blue), and (iv) C_{60} side (region4, orange). While the Li atoms can interact with either only CNT in region1 or only C_{60} in region3 and region4, they can interact with both CNT and C_{60} simultaneously in region2. After defining the four regions, we simulated the adsorption of one Li atom on various positions at each region around the CNT-C_{60} hybrid system. In this study, we placed the Li atom on the following sites: (i) the center of the hexagon sites (Center) of CNT because "Center" has the lowest Li adsorption energy among the sites on the CNT surface, such as top of the carbon atom (Top), above the axial (Axial) or zigzag (Zigzag) carbon−carbon bond (Figure 2d), and (ii) the pentagon and hexagon site of C_{60} because these sites attain the most stable Li adsorption in the C_{60}.

A Li atom is adsorbed on the CNT (from Pos1_CNT@hybrid to Pos10_CNT@hybrid, as shown in Supporting Information Figure 1a,b) and on the C_{60} (from Pos1_C_{60}@hybrid to Pos8_C_{60}@hybrid, as shown in Supporting Information Figure 1c,d). By performing geometry optimization for each adsorption position, we obtained the stable structures (Figure 3a−d) and their corresponding adsorption energies (Table 2). For the CNT@hybrid sites, it seems that the adsorption energy of the Li in region2 becomes relatively lower in comparison to other regions. We think that this is because the Li atom is exposed to C_{60} as well as CNT and has interactions with both components. For the C_{60}@hybrid sites, it is found that the Li adsorption energy has the lowest value (−2.649 eV) in the middle of the C_{60}s (region3). Such strong Li adsorption in region3 is also attributed to the interaction with C_{60}, so we can conclude that the Li adsorption becomes stronger as the Li atom is placed closer to the C_{60}.

On the other hand, region1 has relatively weak Li adsorption (−1.797 eV) because the Li atom is located in the blind site from the C_{60}, even though the adsorption energy in region1 is still lower than that on the bare SWCNT system (−1.720 eV). Considering that the Li adsorption energy in region4 also has a relatively lower value (−2.110 eV), we believe that Li atoms will favorably occupy the C_{60} sites first, especially the mid-space between C_{60}s or between C_{60} and CNT and then the remaining side of C_{60} and CNT sites in order. Through this adsorption, the charge transfer from the adsorbed Li to the CNT-C_{60} hybrid system takes place, and its amount ranges from 0.825*e* to 0.975*e*, depending on the positions.

We also performed an energy decomposition analysis to distinguish the contributions of electrostatic (ES) and nonelectrostatic (NES) interactions to the adsorption energy. The electrostatic energy (Es) was calculated from a point charge model. The nonelectrostatic energy (E_{NES}) was obtained from the difference between the Li adsorption energy and the electrostatic energy (Es) ($E_{NES} = \Delta E_{adsorption} - E_{ES}$). It is clearly shown in Table 3 that the electrostatic interaction is dominant in the Li adsorption on the CNT-C_{60} system. The positive values of E_{NES} indicate that the Li−C distances are too short for dispersive interaction, which is actually in the range of repulsive interaction. This negative electrostatic energy with such short Li−C distances confirms that the nature of Li adsorption on the CNT-C_{60} system is a chemi-sorption through charge transfer.

3.2. Adsorption of Two Li Atoms on CNT-C_{60} Hybrid System. We added another Li atom at various sites in each region near the first Li atom to investigate the Li adsorption mechanism. Once again, it is very important to understand how efficiently Li atoms can utilize the vast amount of surface provided by the hybrid system because the energy density is determined by the number of Li atoms on the electrode. For this purpose, we provided the second Li atom in relation to the first Li atom in each region of the hybrid system, although it is not easy to explicitly define all the possible configurations for accommodating two Li atoms. Thus, we selected the positions for the second Li atom (blue) based on the adsorption energy of the first

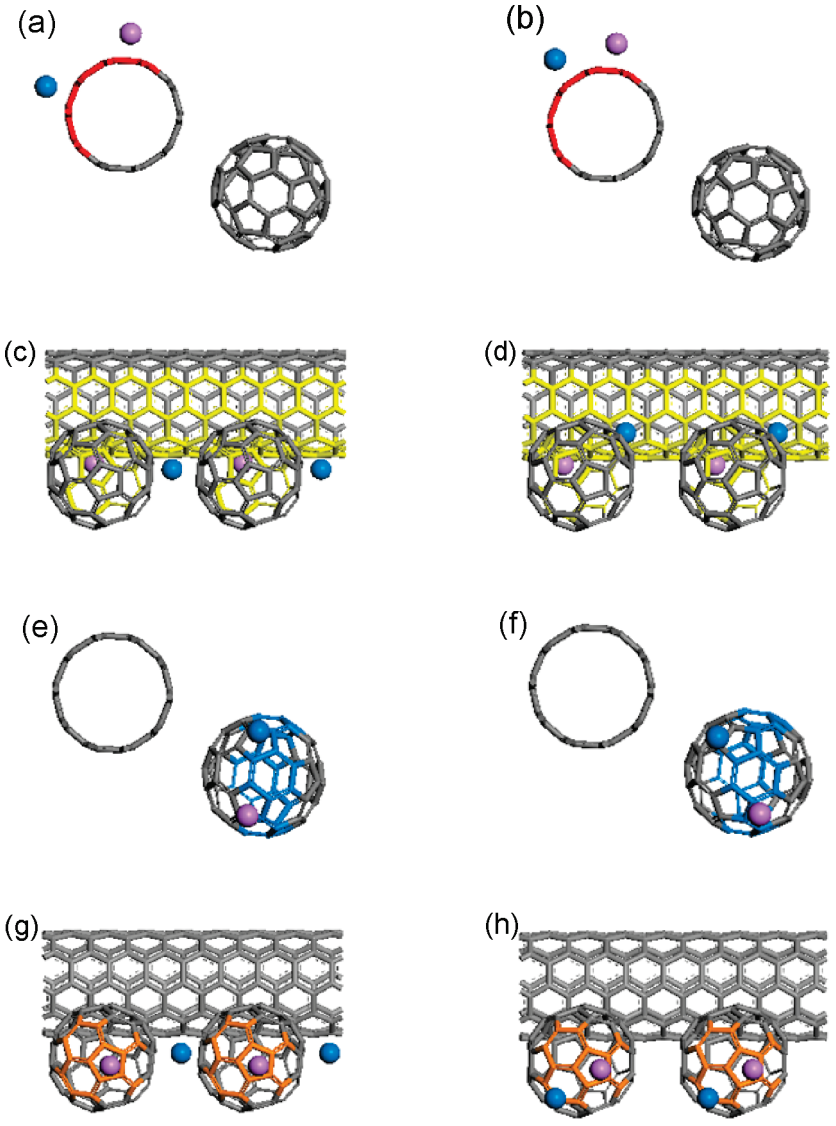

Figure 4. Two-Li adsorption on various regions. For region1: (a) next nearest neighboring (N.N.N.) site; (b) nearest neighboring (N.N.) site to radial direction at CNT@hybrid. For region2: (c) next nearest neighboring (N.N.N.) site; (d) nearest neighboring (N.N.) site to axial direction at CNT:C_{60} middle. For region3: (e) next nearest neighboring (N.N.N.) site; (f) nearest neighboring (N.N.) site to radial direction at C_{60}@hybrid. For region4: (g) next nearest neighboring (N.N.N.) site; (h) nearest neighboring (N.N.) site to axial direction at C_{60}@hybrid.

atom (purple). Here, we assumed that the second Li atom is adsorbed on the nearest neighboring (N.N.) site or the next nearest neighboring (N.N.N.) site in either the radial or axial direction along the axis of the CNT surface for the CNT@hybrid (Supporting Information Figure 2a). We also assumed that the second Li atom is adsorbed on the pentagonal or hexagonal ring in the C_{60}@hybrid in either direction along the axis of the CNT, in the N.N., or the N.N.N. configuration (Supporting Information Figure 2b).

The Li adsorption energies of the two Li atoms using eq 1 are listed in Table 4, and some representative arrangements in each region are displayed in Figure 4. Figure 4a,b shows the optimized structures in region1 representing the N.N.N. and the N.N. site in the radial direction from the first Li atom positioned at Pos1_CNT@hybrid, respectively, and the adsorption energy at the N.N.N. site (Figure 4a, −1.670 eV) is the lowest among the other configurations in region1. Although these values are higher than that of the one-Li adsorption energy, they are still lower than the Li−Li binding energy (experiment: −1.030 eV;[50] Dmol^3: −1.008 eV[42]), which means that the second Li atom prefers adsorption on the hybrid system rather than binding with the given Li atom. Please note that the adsorption energy in region1 is the highest because those Li atoms are not able to interact with C_{60}. On the other hand, the Li adsorption on the C_{60}@hybrid in region4 seems to be more sensitive to the adsorption site (Figure 4g,h); the adsorption energy of the second Li atom is calculated as −2.312 eV for the pentagonal site (Figure 4g, the N.N.N. site of the pentagonal site) and −1.839 eV for the hexagonal site (Figure 4h, the N.N. site of the pentagonal site) in the axial direction starting from the Pos7_C_{60}@hybrid, which seems to suggest that the Li adsorption will take place using the N.N.N. sites of the pentagon site for C_{60}.

The Li adsorption energies in region2 (Figure 4c,d) show low values, from −2.188 eV (at the N.N.N. site in the radial direction

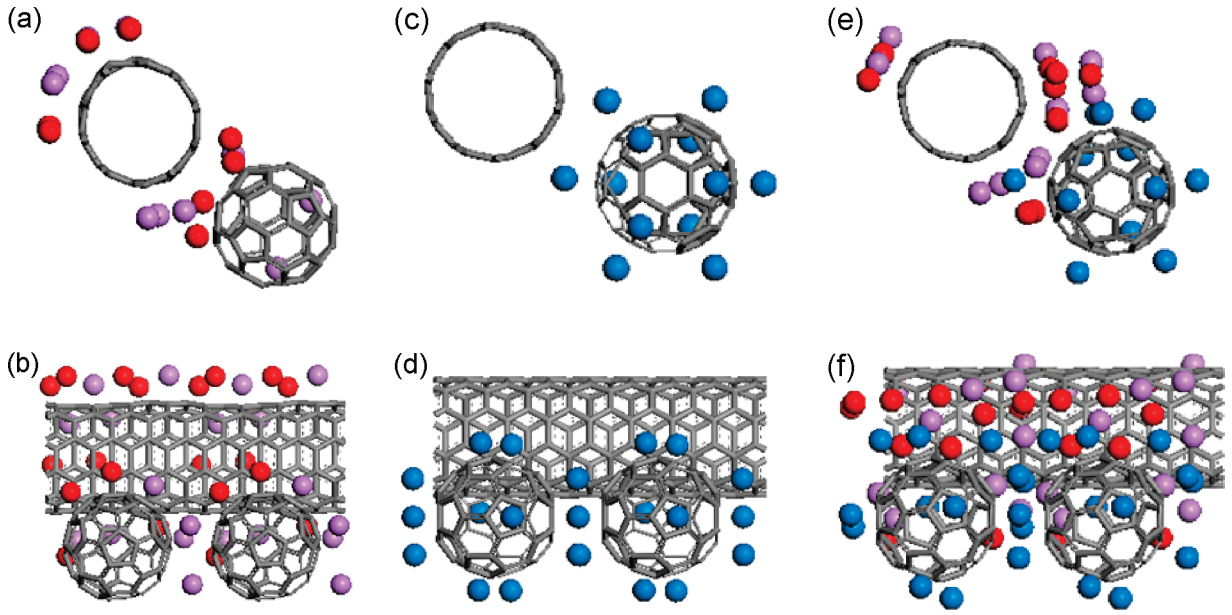

Figure 5. Front and side view of multiple-Li adsorption on the (5,5) CNT-C_{60} hybrid system: (a, b) 20 Li atoms on the CNT@hybrid; (c, d) 12 Li atoms on the C_{60}@hybrid; (e, f) 32 Li atoms on the CNT-C_{60} system.

from the first Li atom at Pos8_CNT@hybrid) to −2.632 eV (at the N.N.N. site in the axial direction from Pos1_C_{60}@hybrid, Figure 4c). In region2, the interaction with both CNT and C_{60} enhances the Li adsorption on the hybrid system, while it seems Li adsorption does not depend on the adsorption sites within this region, compared to region1 and region4. The Li adsorption energy in region3 is also low: −2.601 eV at the N.N.N. site and −2.623 eV at the N.N. site in the radial direction from the first atom at the Pos3_C_{60}@hybrid (Figure 4e,f). For both cases, the adsorption energy is low because the Li atoms are located between C_{60}s which have strong electron affinity. From the calculation results, we could expect that Li adsorption starting from around C_{60} will proceed in the direction that maximizes the exposure to C_{60} of high electron affinity.

3.3. Multiple Li Atoms Adsorbed on CNT-C_{60} Hybrid System. Finally, multiple Li atoms cover the surface of the CNT-C_{60} hybrid system through adsorption on the preferred N.N.N. sites. The number of absorbed Li atoms is 20 for CNT@hybrid and 12 for C_{60}@hybrid; therefore, a total of 32 Li atoms wrap up the hybrid system. The initial structure is presented in the Supporting Information Figure 3. After the geometry optimization, the positions of the Li atoms are adjusted as shown in Figure 5a−f. From the optimized structures displayed, it is observed that the Li atoms that initially attached on the CNT@hybrid sites (Figure 5a,e) are attracted to C_{60}, while the Li atoms around C_{60}, as shown in the Figure 5c,e, keep their original positions because the C_{60} sites have lower Li adsorption energies than the CNT sites. Such positional adjustment agrees well with the results observed for the two-Li system, showing the lowest Li adsorption energy around C_{60}, which drives Li atoms from the CNT sites toward C_{60}. The adsorption energies for the multiple Li adsorption are −1.745 eV for CNT@hybrid and −2.147 eV for C_{60}@hybrid, indicating that the Li adsorption will take place on the C_{60} side first (especially starting from the sites between CNT and C_{60}) until all the available sites on the C_{60} side are consumed, and the Li adsorption will subsequently proceed to the sites on the CNT side. Although the Li adsorption energy decreases with increasing numbers of Li atoms, all these adsorption energies are lower than the Li−Li binding energy, indicating that the Li cluster formation is not likely to occur until all available sites on the CNT-C_{60} hybrid system are covered.

3.4. Electronic Properties of the CNT-C_{60} Hybrid System. We investigated electronic properties as a function of the number of Li atoms on the CNT-C_{60} hybrid system in order to analyze the effect of Li adsorption. Figure 6a−g shows the highest occupied molecular orbital (HOMO) and the lowest unoccupied molecular orbital (LUMO) of some of the systems: one Li atom (Figure 6b−d) and many Li atoms around the hybrid system (Figure 6e−g). In the pristine hybrid system shown in Figure 6a, the HOMO is primarily formed on the CNT side, while the LUMO is on the C_{60} side. For the molecular orbital of the one Li atom systems, such as CNT@hybrid (Figure 6b), CNT:C_{60} middle (Figure 6c), and C_{60}@hybrid (Figure 6d), the LUMO is mostly formed at the components that are close to a Li atom depending on the Li position. It should be noted, however, that the overall feature of the molecular orbital is dominated by the CNT-C_{60} system. Thus, the energy levels of the HOMO and LUMO for one-Li systems (Figure 6b−d) are somehow similar to those of the pure CNT-C_{60} hybrid system without Li (Figure 6a).

On the other hand, when many Li atoms are adsorbed (Figure 6e−g), the molecular orbitals are mostly governed by the Li atoms, so the energy levels and distribution of the HOMO and LUMO for the multiple Li adsorption systems undergo significant changes compared to those for the pure CNT-C_{60} hybrid system. Additionally, the HOMO−LUMO difference is seriously reduced; the average differences are 1.331 and 0.195 eV for the one Li atom system and the multiple Li atom system, respectively. This result indicates that, as the number of adsorbed Li atoms increases, the CNT-C_{60} hybrid system is more metalized, and its electronic structure becomes more polarizable due to the decreasing electronic hardness. Thus, we expect that electrons can easily flow through the hybrid system.

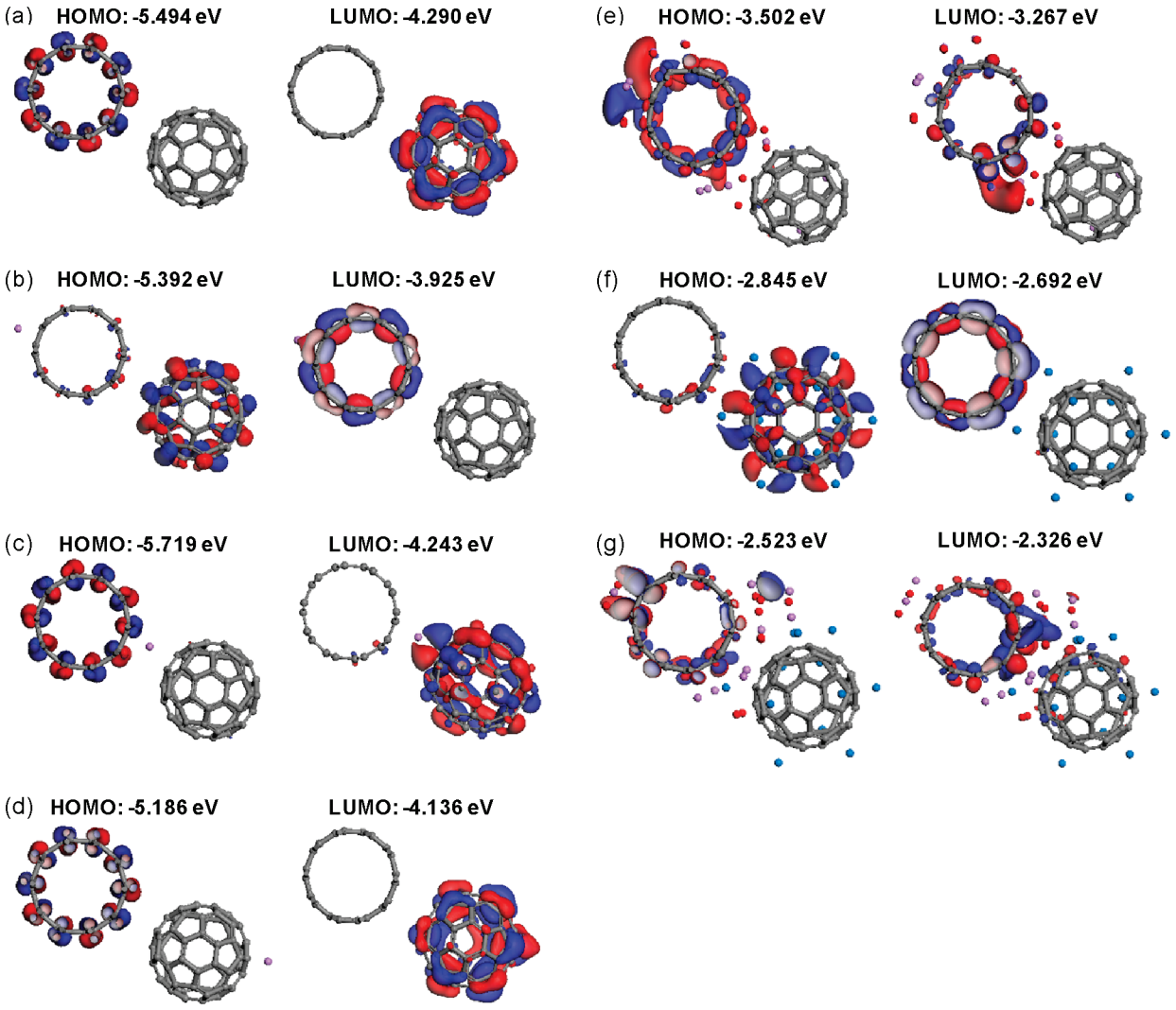

Figure 6. HOMO and LUMO of the CNT-C_{60} hybrid systems at different numbers of Li atoms: (a) no Li on the system; one Li atom (b) on the CNT side; (c) between CNT and C_{60}; (d) on the C_{60} side; (e) 20 Li atoms around CNT; (f) 12 Li atoms around C_{60}; (g) 32 Li atoms around CNT and C_{60}. (The isovalue of the HOMO and LUMO surface is 0.02.)

4. CONCLUSION

The mechanism of adsorption of Li onto a new type of hybrid system consisting of CNT and C_{60} was investigated using the first-principles method. We found that the charge transfer takes place from CNT to C_{60} due to the high electron affinity of C_{60}, so that CNT has a positive charge and C_{60} has a negative charge in the hybrid system. This positively charged CNT could achieve lower Li adsorption energy (−2.571 eV) than the bare CNT system (−1.720 eV), which indicates that the CNT-C_{60} hybrid system has better Li adsorption capability compared to the bare CNT.

Analyzing the Li adsorption as a function of various regions in the CNT-C_{60} hybrid system, we found that the Li adsorption will occur preferentially on the C_{60} side, more specifically on the mid-space between C_{60}s (region3) or between CNT and C_{60} (region2), and then subsequently proceed toward the CNT side instead of forming a Li cluster because the Li−C adsorptive interaction (e.g., −2.138 eV in overall average for the two Li system) is more stable than the Li−Li binding interaction (−1.030 eV). The change in the electronic properties of the hybrid system was also investigated as a function of the number of Li atoms. From this calculation, it was found that the HOMO−LUMO gap decreased and electron distribution around Fermi level increased concurrently, which means that the system becomes more metalized as the number of Li atoms in the hybrid system increases. Therefore, it is to be expected that the CNT-C_{60} hybrid system has enhanced conductivity and superior Li adsorption capability compared to the bare CNT system.

■ ASSOCIATED CONTENT

Supporting Information. Figures of initial structures of one-Li adsorption on various positions around CNT@hybrid; the radial and axial direction of the second Li atom adsorption on the two-Li atom system around CNT@hybrid and C60@hybrid; and front and side views of multiple-Li adsorption on the CNT-C_{60} hybrid system. This material is available free of charge via the Internet at http://pubs.acs.org..

AUTHOR INFORMATION

Corresponding Author
*E-mail: SeungSoon.Jang@mse.gatech.edu. Phone: 404-385-3356. Fax: 404-894-9140.

ACKNOWLEDGMENT

K.D. is supported by Summer Undergraduate Research Fellowship (SURF) 2010, sponsored by National Science Foundation Research Experiences for Undergraduates (NSF REU) program (DMR-0851574).

REFERENCES

(1) Postma, H. W. C.; Teepen, T.; Yao, Z.; Grifoni, M.; Dekker, C. *Science* **2001**, *293*, 76–79.
(2) Novoselov, K. S.; Geim, A. K.; Morozov, S. V.; Jiang, D.; Zhang, Y.; Dubonos, S. V.; Grigorieva, I. V.; Firsov, A. A. *Science* **2004**, *306*, 666–669.
(3) Baughman, R. H.; Zakhidov, A. A.; de Heer, W. A. *Science* **2002**, *297*, 787–792.
(4) Kong, J.; Franklin, N. R.; Zhou, C.; Chapline, M. G.; Peng, S.; Cho, K.; Dai, H. *Science* **2000**, *287*, 622–625.
(5) Tarascon, J. M.; Armand, M. *Nature* **2001**, *414*, 359–367.
(6) Dahn, J. R.; Zheng, T.; Liu, Y. H.; Xue, J. S. *Science* **1995**, *270*, 590–593.
(7) Bellucci, S. *Phys. Status Solidi C* **2005**, *2*, 34–47.
(8) Hong, S.; Myung, S. *Nat. Nanotechnol.* **2007**, *2*, 207–208.
(9) Yu, M.-F.; Lourie, O.; Dyer, M. J.; Moloni, K.; Kelly, T. F.; Ruoff, R. S. *Science* **2000**, *287*, 637–640.
(10) Nalimova, V. A.; Sklovsky, D. E.; Bondarenko, G. N.; Alvergnat-Gaucher, H.; Bonnamy, S.; Béguin, F. *Synth. Met.* **1997**, *88*, 89–93.
(11) Che, G.; Lakshmi, B. B.; Fisher, E. R.; Martin, C. R. *Nature* **1998**, *393*, 346–349.
(12) Maurin, G.; Bousquet, C.; Henn, F.; Bernier, P.; Almairac, R.; Simon, B. *Chem. Phys. Lett.* **1999**, *312*, 14–18.
(13) Dubot, P.; Cenedese, P. *Phys. Rev. B* **2001**, *6324*, 241402.
(14) Zhao, J.; Buldum, A.; Han, J.; Ping, Lu, J. *Phys. Rev. Lett.* **2000**, *85*, 1706.
(15) Kar, T.; Pattanayak, J.; Scheiner, S. *J. Phys. Chem. A* **2001**, *105*, 10397–10403.
(16) Yang, J.; Liu, H. J.; Chan, C. T. *Phys. Rev. B* **2001**, *64*, 085420.
(17) Duclaux, L. *Carbon* **2002**, *40*, 1751–1764.
(18) Liu, Y.; Yukawa, H.; Morinaga, M. *Comput. Mater. Sci.* **2004**, *30*, 50–56.
(19) Udomvech, A.; Kerdcharoen, T.; Osotchan, T. *Chem. Phys. Lett.* **2005**, *406*, 161–166.
(20) Zhao, M. W.; Xia, Y. Y.; Liu, X. D.; Tan, Z. Y.; Huang, B. D.; Li, F.; Ji, Y. J.; Song, C. *Phys. Lett. A* **2005**, *340*, 434–439.
(21) Khantha, M.; Cordero, N. A.; Alonso, J. A.; Cawkwell, M.; Girifalco, L. A. *Phys. Rev. B* **2008**, *78*, 115430.
(22) Meunier, V.; Kephart, J.; Roland, C.; Bernholc, J. *Phys. Rev. Lett.* **2002**, *88*, 075506.
(23) Garau, C.; Frontera, A.; Quinonero, D.; Costa, A.; Ballester, P.; Deya, P. M. *Chem. Phys. Lett.* **2003**, *374*, 548–555.
(24) Zhao, M.; Xia, Y.; Mei, L. *Phys. Rev. B* **2005**, *71*, 165413.
(25) Nishidate, K.; Hasegawa, M. *Phys. Rev. B* **2005**, *71*, 245418.
(26) Gao, B.; Kleinhammes, A.; Tang, X. P.; Bower, C.; Fleming, L.; Wu, Y.; Zhou, O. *Chem. Phys. Lett.* **1999**, *307*, 153–157.
(27) Claye, A. S.; Fischer, J. E.; Huffman, C. B.; Rinzler, A. G.; Smalley, R. E. *J. Electrochem. Soc.* **2000**, *147*, 2845–2852.
(28) Zhou, Z.; Gao, X. P.; Yan, J.; Song, D. Y.; Morinaga, M. *J. Phys. Chem. B* **2004**, *108*, 9023–9026.
(29) Zhou, Z.; Zhao, J. J.; Gao, X. P.; Chen, Z. F.; Yan, J.; Schleyer, P. V.; Morinaga, M. *Chem. Mater.* **2005**, *17*, 992–1000.
(30) Shimoda, H.; Gao, B.; Tang, X. P.; Kleinhammes, A.; Fleming, L.; Wu, Y.; Zhou, O. *Phys. Rev. Lett.* **2001**, *88*, 015502.
(31) Gao, B.; Bower, C.; Lorentzen, J. D.; Fleming, L.; Kleinhammes, A.; Tang, X. P.; McNeil, L. E.; Wu, Y.; Zhou, O. *Chem. Phys. Lett.* **2000**, *327*, 69–75.
(32) Arai, M.; Utsumi, S.; Kanamaru, M.; Urita, K.; Fujimori, T.; Yoshizawa, N.; Noguchi, D.; Nishiyama, K.; Hattori, Y.; Okino, F.; Ohba, T.; Tanaka, H.; Kanoh, H.; Kaneko, K. *Nano Lett.* **2009**, *9*, 3694–3698.
(33) Smith, B. W.; Monthioux, M.; Luzzi, D. E. *Nature* **1998**, *396*, 323–324.
(34) Okada, S.; Saito, S.; Oshiyama, A. *Phys. Rev. Lett.* **2001**, *86*, 3835–3838.
(35) Kawasaki, S.; Mai, Y.; Hirose, M. *Mater. Res. Bull.* **2009**, *44*, 415–417.
(36) Nasibulin, A. G.; Pikhitsa, P. V.; Jiang, H.; Brown, D. P.; Krasheninnikov, A. V.; Anisimov, A. S.; Queipo, P.; Moisala, A.; Gonzalez, D.; Lientschnig, G.; Hassanien, A.; Shandakov, S. D.; Lolli, G.; Resasco, D. E.; Choi, M.; Tomanek, D.; Kauppinen, E. I. *Nat. Nano* **2007**, *2*, 156–161.
(37) Meng, T.; Wang, C.-Y.; Wang, S.-Y. *Phys. Rev. B* **2008**, *77*, 033415.
(38) Li, C.; Chen, Y. H.; Wang, Y. B.; Iqbal, Z.; Chhowalla, M.; Mitra, S. *J. Mater. Chem.* **2007**, *17*, 2406–2411.
(39) Li, C.; Mitra, S. *Appl. Phys. Lett.* **2007**, *91*, 253112–3.
(40) Li, Y. F.; Kaneko, T.; Hatakeyama, R. *Nanotechnology* **2008**, *19*, 415201.
(41) Perdew, J. P.; Burke, K.; Ernzerhof, M. *Phys. Rev. Lett.* **1996**, *77*, 3865–3868.
(42) Perdew, J. P.; Burke, K.; Wang, Y. *Phys. Rev. B* **1996**, *54*, 16533.
(43) Delley, B. *J. Chem. Phys.* **1990**, *92*, 508–517.
(44) Delley, B. *J. Chem. Phys.* **2000**, *113*, 7756–7764.
(45) Monkhorst, H. J.; Pack, J. D. *Phys. Rev. B* **1976**, *13*, 5188–5192.
(46) Mulliken, R. S. *J. Chem. Phys.* **1955**, *23*, 2338–2342.
(47) Segall, M. D.; Pickard, C. J.; Shah, R.; Payne, M. C. *Mol. Phys.* **1996**, *89*, 571–577.
(48) Koh, W.; Choi, J. I.; Lee, S. G.; Lee, W. R.; Jang, S. S. *Carbon* **2011**, *49*, 286–293.
(49) Sun, Q.; Jena, P.; Wang, Q.; Marquez, M. *J. Am. Chem. Soc.* **2006**, *128*, 9741–9745.
(50) K.P. Huber G. H. *Constants of Diatomic Molecules*; Van Nostrand Reinhold: New York, NY, 1979.